UTa$_2$O(S$_2$)$_3$Cl$_6$: A ribbon structure containing a heterobimetallic 5d–5f M$_3$ cluster

Daniel M. Wells [a], George H. Chan [a], Donald E. Ellis [a,b], James A. Ibers [a,*]

[a] Department of Chemistry, Northwestern University, 2145 Sheridan Road, Evanston, IL 60208-3113, USA
[b] Department of Physics and Astronomy, Northwestern University, 2145 Sheridan Road, Evanston, IL 60208-3113, USA

ARTICLE INFO

ABSTRACT

A new solid-state compound containing a heterobimetallic cluster of U and Ta, UTa$_2$O(S$_2$)$_3$Cl$_6$, has been synthesized and its structure has been characterized by single-crystal X-ray diffraction methods. UTa$_2$O(S$_2$)$_3$Cl$_6$ was synthesized from UCl$_4$ and Ta$_{1.2}$S$_2$ at 883 K. The O is believed to have originated in the Ta$_{1.2}$S$_2$ reactant. The compound crystallizes in the space group $P\bar{1}$ of the triclinic system. The structure comprises a UTa$_2$ unit bridged by μ_2-S$_2$ and μ_3-O groups. Each Ta atom bonds to two μ_2-S$_2$, the μ_3-O, and two terminal Cl atoms. Each U atom bonds to two μ_2-S$_2$, the μ_3-O, and four Cl atoms. The Cl atoms bridge in pairs to neighboring U atoms to form a ribbon structure. The bond distances are normal and are consistent with formal oxidation states of +IV/+V/−II/−I/−I for U/Ta/O/S/Cl, respectively. The optical absorbance spectrum displays characteristic transition peaks near the absorption edge. Density functional theory was used to assign these peaks to transitions between S^{1-} valence-band states and empty U 5f–6d hybrid bands. Density-of-states analysis shows overlap between Ta 5d and U bands, consistent with metal–metal interactions.

1. Introduction

Trimetallic cluster compounds that contain bridging μ_3-oxo and dichalcogenido ligands are well established in organometallic chemistry [1–3]. However, none of these compounds contains U. The few trimetallic clusters that contain U involve OCMe$_3$ [4], hexadentate Schiff base [5], or multiple μ_2-I ligands [6]. Several other multimetallic molecular compounds involving U are known where large ligands allow for binding to multiple metals or the U atoms are bridged by multidentate ligands [7–9]. Examples of trinuclear Ta complexes are also rare compared to those involving neighboring Mo or W atoms. Those known Ta complexes contain bridging μ_2-O [10–12] rather than μ_2-S$_2$ ligands found here and are common for Mo and W. Most of the three-center-hetero-metallic complexes that have been synthesized contain multiple μ_3-S ligands [13,14]. Compounds containing both 5d-transition metals and 5f-actinides and a chalcogen (S, Se, or Te) are also rare [15]. In the U/Ta system there appear to be no examples.

Several years ago we began to investigate the use of UCl$_4$ in the high-temperature syntheses of new solid-state uranium transition-metal chalcogenides. Although we have subsequently successfully used UCl$_4$ in metathesis reactions [16], initially we explored the types of products that we could obtain with UCl$_4$ in the presence of various transition-metal chalcogenides where no

metathesis was expected. One such reaction involved TaS$_2$; the results of that reaction are described here where we present the crystal structure, optical absorption spectrum, and density functional theory analysis of the compound UTa$_2$O(S$_2$)$_3$Cl$_6$ whose crystal structure contains a heterobimetallic cluster.

2. Experimental

2.1. Synthesis

UCl$_4$ was prepared by a modification [16] of a literature procedure [17]. TaS$_2$ (Johnson Matthey, 99.8%), denoted herein as the old lot, had resided in this laboratory for an unknown number of years. TaS$_2$ (Alfa, 99.8%), denoted herein as the new lot, was used as supplied.

A mixture of UCl$_4$ (0.105 mmol) and TaS$_2$ (old lot, 0.168 mmol) was loaded into a fused-silica tube that was then evacuated and sealed. The tube was heated in a computer-controlled furnace to 373 K in 2 h, heated to 883 K in 99 h, held at 883 K for 24 h, slow cooled at 4.1 K/h to 473 K, and then slow cooled at 4.9 K/h to 293 K. The product consisted of small orange needles of what turned out to be UTa$_2$O(S$_2$)$_3$Cl$_6$ in approximately 40% yield. Even though the yield was relatively high, almost all of these air-sensitive crystals were imbedded in a dark brown residual powder. Analysis by powder X-ray diffraction and EDS methods indicated that the byproducts were unreacted UCl$_4$ and TaS$_2$

* Corresponding author. Fax: +1 847 491 2976.
E-mail address: ibers@chem.northwestern.edu (J.A. Ibers).

polymorphs. The reaction tube was not etched. Therefore, the fused-silica was not the source of O in $UTa_2O(S_2)_3Cl_6$.

2.2. Structure determination

Single-crystal X-ray diffraction data were collected with the use of graphite-monochromatized Mo Kα radiation ($\lambda=0.71073$ Å) at 153 K on a Bruker Smart-1000 CCD diffractometer [18]. The crystal-to-detector distance was 5.023 cm. Crystal decay was monitored by re-collecting 50 initial frames at the end of data collection. Data were collected by a scan of 0.3° in ω in groups of 606 frames at φ settings of 0°, 90°, 180°, and 270°. The exposure time was 15 s/frame. The collection of the intensity data was carried out with the program SMART [18]. Cell refinement and data reduction were carried out with the use of the program APEX2 [19]. A Leitz microscope equipped with a calibrated traveling micrometer eyepiece was employed to measure accurately the crystal dimensions. Face-indexed absorption, incident beam, and decay corrections were performed numerically with the use of the program SADABS [18].

The structure was solved with the direct-methods program SHELXS and refined with the least-squares program SHELXL [20]. After the U, Ta, S, and Cl atoms had been located and their positions refined, there remained a residual peak in the difference electron density synthesis that was located about 0.6 Å below the UTa_2 plane. When this peak was assigned to O and then the O atom was included in the refinements, reasonable displacement parameters and normal U–O and Ta–O distances resulted. The program STRUCTURE TIDY [21] was then employed to standardize the atomic coordinates. Additional experimental details are given in Table 1 and the Supporting material. Selected metrical data are given in Table 2.

2.3. Single-crystal optical measurements

Absorption measurements with unpolarized and polarized light were performed over the range 400 nm (3.10 eV) to 900 nm (1.38 eV) and analyzed by methods previously described [22]. The dimensions of the crystal were not measured.

2.4. Powder X-ray diffraction measurements

Powder X-ray diffraction data from CuKα radiation ($\lambda=1.54056$ Å) were collected between 5 and 80° 2θ on a Rigaku Geigerflex automatic

Table 1
Crystal data and structure refinement for $UTa_2O(S_2)_3Cl_6$.

Formula mass	1020.99
Space group	$P\bar{1}$
a (Å)	6.844 (1)
b (Å)	9.435 (1)
c (Å)	12.628 (2)
α (°)	84.749 (2)
β (°)	82.721 (2)
γ (°)	89.500 (2)
V (Å³)	805.4 (2)
ρ_c (g cm⁻³)	4.210
T (K)	153(2)
Z	2
μ (cm⁻¹)	253.27 (MoKα)
R(F)ᵃ	0.0389
$R_w(F^2)$ᵇ	0.0907

ᵃ $R(F)=\Sigma||F_o|-|F_c||/\Sigma|F_o|$ for $F_o^2>2\sigma(F_o^2)$.
ᵇ $R_w(F_o^2)=\{\Sigma[w(F_o^2-F_c^2)^2]/\Sigma wF_o^4\}^{1/2}$ for all data. $w^{-1}=\sigma^2(F_o^2)+(0.0361F_o^2)^2$ for $F_o^2\geq0$; $w^{-1}=\sigma^2(F_o^2)$ for $F_o^2<0$.

Table 2
Selected interatomic distances (Å) in $UTa_2O(S_2)_3Cl_6$.

U1–O1	2.297 (7)	Ta1–S4	2.569 (3)
U1–Cl1	2.759 (3)	Ta2–O1	1.979 (7)
U1–Cl2	2.766 (3)	Ta2–Cl5	2.291 (3)
U1–Cl1	2.805 (3)	Ta2–Cl6	2.367 (3)
U1–S1	2.819 (3)	Ta2–S5	2.439 (3)
U1–S5	2.859 (3)	Ta2–S6	2.451 (3)
U1–S2	2.912 (3)	Ta2–S3	2.508 (3)
U1–S6	2.928 (3)	Ta2–S4	2.570 (3)
Ta1–O1	2.013 (7)	S1–S2	2.081 (4)
Ta1–Cl3	2.299 (3)	S3–S4	2.077 (4)
Ta1–Cl4	2.336 (3)	S5–S6	2.081 (4)
Ta1–S2	2.432 (3)	U1–Ta1	3.5882 (8)
Ta1–S1	2.481 (3)	U1–Ta2	3.5986 (8)
Ta1–S3	2.530 (3)	Ta1–Ta2	3.2972 (7)

powder diffraction instrument. All powder diffraction data were analyzed with the use of the program JADE 8 [23].

2.5. Computational details

Periodic spin-polarized band structure calculations were performed with the use of the first principles DFT program VASP (Vienna ab initio simulation package); pseudopotentials were applied with a plane-wave basis [24–27]. The exchange-correlation potential was chosen as the generalized gradient approximation (GGA) in a projector augmented wave (PAW) method [28]. The onsite Coulomb correction to the uranium 5f shell, that is the Hubbard U [29] term, was implemented in the rotationally invariant approach where the onsite Coulomb term U and onsite exchange term J were treated together as $U_{eff}=U-J$ [30]. Because the Coulomb correction in this method is a simple addition to the total energy expression, it has limited effect on the atomic positions and was only included in final electronic self-consistent calculations. The value of U_{eff} was determined by fitting the peaks in the density-of-states (DOS) and band gap, E_g, to the experimentally determined optical spectrum. The optimum value of U_{eff} was determined by minimizing the root-sum-squares of the differences for the two peaks and E_g.

All magnetic-structure energy comparisons, U_{eff} fitting, and final calculations included spin orbit coupling (SOC), as the effects of SOC can be very large for 5f orbitals and are known to shift their energies greatly. SOC couples the magnetic spin polarization to the lattice; therefore a direction of magnetization must be chosen. [001] was taken throughout as the direction of magnetization, and magnetic anisotropy was not investigated. The direction of magnetization will have little effect on the DOS and band overlap investigated here. Automatically generated Monkhorst–Pack grids were used to carry out Brillouin zone integrations [31]. $4\times4\times2$ k-point meshes were chosen for relaxations and total energy calculations; these were increased to $6\times6\times2$ k-point meshes to establish convergence, for energy comparisons, U_{eff} fitting, and DOS analysis. Ionic relaxation convergence was established when Hellmann–Feynmann forces on each ion relaxed below 0.02 eV/Å.

In the calculations the electrons described as core in the PAW potentials were those composed of [Xe] $5d^{10}4f^{14}$ for U, leaving 14 valence elections per atom as $5f^36s^2p^6d^17s^2$; [Xe] for Ta, leaving 11 valence electrons per atom as $6s^25p^65d^3$; [Ne] for S, leaving six valence electrons as $3s^22p^4$; [He] for O, leaving six valence electrons as $2s^2p^4$; and [Ne] for Cl, leaving seven electrons as $3s^2p^5$. Calculations were conducted on the 32-atom periodic crystallographic unit cell in the triclinic space group $P\bar{1}$; atomic positions within the fixed 153 K unit cell were relaxed to their

lowest energy positions before SOC and an onsite Coulomb correction were applied. Because the magnetic properties of $UTa_2O(S_2)_3Cl_6$ are unknown and the unit cell contains two U atoms, both the antiferromagnetic and ferromagnetic structures were relaxed and the final energies were compared. An onsite Coulomb correction was not used at this point because U_{eff} would change depending upon magnetic polarization. Hence, comparisons between calculations with different values of U_{eff} would be meaningless. Charge balance in the structure suggested tetravalent U ($5f^2$) and nonmagnetic pentavalent Ta ($5d^0$); however, magnetic moments on the Ta centers, though initially set to 0, were not constrained.

For analysis purposes charge density within the cell was divided into atomic spheres of Wigner–Seitz radii, R_{WS}. These were initially set to the standard radii [32] and then increased to fill the unit-cell volume. Final values of R_{WS} were 1.35, 0.90, 1.50, 1.80, and 2.00 Å for U, Ta, O, S, and Cl, respectively. Even though the Bader topological method [33] has been used with success in some systems, we have found that it does not predict oxidation states in others [34]. Often there is some covalent bonding around U(IV) centers; as a result the Bader method finds electron-density-zero-flux surfaces between the bonded atoms and very little charge transfer. Therefore, only the R_{WS} method was applied here. Calculated oxidation states here are defined as the PAW valence minus the final relaxed R_{WS} charge.

3. Results and discussion

3.1. Synthesis

Air-sensitive orange crystals of $UTa_2O(S_2)_3Cl_6$ were synthesized in approximately 40% yield from the reaction of UCl_4 with TaS_2 (old lot) in a 1:1.6 molar ratio. Almost all of these crystals were imbedded in a brown residual mass. Only a few that were large enough for a single-crystal X-ray diffraction study could be dislodged.

3.2. The source of oxygen in $UTa_2O(S_2)_3Cl_6$?

The reaction of UCl_4 with TaS_2 cannot lead to the oxygen-containing compound shown in Fig. 1. The assignment of a μ_3-O atom to the electron density at that site is based on the high oxophilicity of U, the reasonable U–O and Ta–O bond distances that ensued, the known $M_3(\mu_3\text{-O})(S_2)_3^-$ type clusters, and the reasonable displacement parameters.

The synthesis of $UTa_2O(S_2)_3Cl_6$, as described above, is repeatable with the old lot of TaS_2. Syntheses with TaS_2 (new lot) and other oxygen sources, including UOS, UO_2, UO_3, and Ta_2O_5, proved to be unsuccessful. TaS_2 (old lot) we characterized by powder diffraction methods as $Ta_{1.2}S_2$, although it is possible that there are some other $6s\text{-}Ta_{1+y}S_2$ compounds present. The many polymorphs of layered TaS_2 differ in Ta:S ratio and Ta coordination environments [35]. Three low-angle peaks were found reasonably close to those corresponding to the 00ℓ peaks from monoclinic Ta_2O_5 [30] and orthorhombic $Ta_{7.30}O_{11.36}$ [36]; however, the amounts of these O-containing compounds could not be quantified. The new lot of TaS_2 was found by powder diffraction methods to contain $Ta_{0.703}O_{1.65}$ [37] and $1s\text{-}TaS_2$ [35,38] in an approximately 1:9 ratio. Even though this new lot contains an oxide, its use in the synthesis did not result in $UTa_2O(S_2)_3Cl_6$ as a product. Thus, it seems likely that there is some other oxygen contamination in the old lot of TaS_2, or the form of the TaS_2 or oxide is critical. Purchase of pure "$Ta_{1.2}S_2$" is unlikely because there are many binary Ta/S polymorphs and the synthesis of a single polymorph is reported to be extremely difficult, especially because annealing increases the amount of $6s\text{-}TaS_2$ [35]. All vendors contacted stated their TaS_2 products contained a mixture of phases.
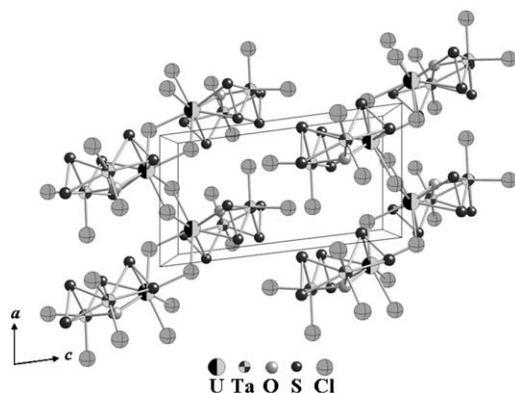
A rough calculation suggests a composition $Ta_{1.2}S_{1.8}O_{0.2}$ would account for the yield of $UTa_2O(S_2)_3Cl_6$. However, there are no known $TaS_{2-x}O_x$ structures and so the calculation of theoretical powder patterns is not possible.

3.3. Structure

The structure (Fig. 1) comprises $UTa_2O(S_2)_3Cl_6$ clusters. Each cluster is connected to two other clusters through four μ_2–Cl atoms to generate a ribbon that propagates along the a-axis. Each cluster (Fig. 2) consists of one U and two Ta atoms bridged by μ_2–S_2^{2-} disulfide units. In addition the heavy atoms share a central μ_3–O atom to form a triangular cluster. The O atom is located 0.57 Å below the UTa_2 plane whereas the S_2^{2-} units are situated so one S atom is about 0.23 Å below the plane and the other about 1.63 Å above the plane. The S–S single bonds are 2.077(4), 2.081(4), and 2.081(4) Å, reasonably close to the range of S–S bonds found in S_8 (2.035(2)–2.060(2) Å) [39]. In addition to four S bonds and one O bond, each Ta atom bonds to two terminal Cl atoms. The terminal Cl atoms are oriented so one is about 0.99 Å above the UTa_2 plane whereas the other is about 2.20 Å below the plane. The structure is similar to that of $Mo_3S_7Cl_4$, but in that structure two Mo atoms of the triangular unit bridge to neighboring moieties and only one of the Mo atoms has terminal Cl atoms [40].

Fig. 1. View down [010] of the structure of $UTa_2O(S_2)_3Cl_6$.
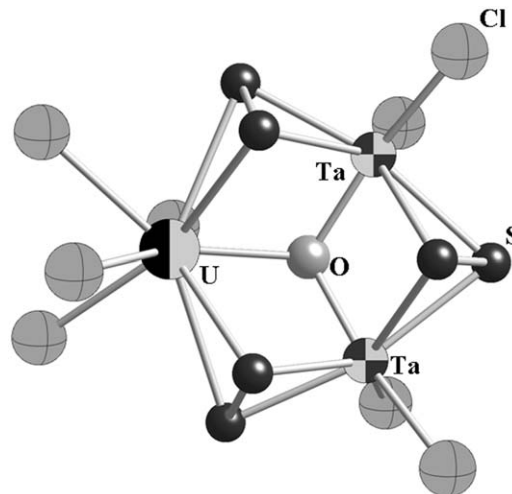
Fig. 2. The $UTa_2O(S_2)_3Cl_6$ cluster with completed coordination sphere around U.

Charge balance may be achieved with the formal oxidation states of +IV for U and +V for Ta.

It is interesting that unintended O contamination is not uncommon and continues to aid in the syntheses of novel solid-state compounds [3,7,41–43].

Selected bond distances and angles may be found in Table 2. The U–Ta interactions of 3.5887(7) and 3.5989(7) Å are reasonable compared to those in U/Ta oxide compounds where they range from 3.468(1) to 3.709(1) Å [44–47]. The Ta–Ta interaction at 3.2977(7) Å is also normal when compared to other $Ta_3(\mu_3–O)$

clusters where the distances range from 3.1185(3) to 3.3378(3) Å [11]. The U–U distances are 4.424 and 4.502 Å, well beyond the Hill limit for $f–f$ overlap (about 3.4 Å) [48].

The other bond distances are also normal. For the U atoms the following comparisons can be made to other six- and eight-coordinate tetravalent U compounds: U–O, 2.298(7) Å vs. 2.27(3) Å in the $\mu_3–O$ in the $U_3(O)(OCMe_3)_{10}$ structure [4]; U–S, 2.819(3)–2.929(3) Å vs. 2.846(2) Å in $K_{0.91}U_{1.79}S_6$ [49]; U–Cl, 2.759(3) to 2.805(3) Å vs. 2.644(2) to 2.889(1) Å in the UCl_4 structure [50]. For Ta the following comparisons can be made to other five-, six-, and eight-coordinate pentavalent Ta compounds: Ta–O, 1.979(7) and 2.013(7) Å vs. 2.058(3)–2.148(3) Å in Ta_3 $(\mu_3–O)$ clusters [11,12]; Ta–S, 2.439(3)–2.570(3) Å vs. 2.540(2) and 2.578(3) in $Ta(PS_4)(S_2)$ [51]; Ta–Cl, 2.291(3)–2.368(3) Å vs. 2.320(1)–2.344(1) for terminal Cl in $Ta_2Cl_8(C_6H_{18}Cl_2N_2PSi_2)_2$ [52].

3.4. Single-crystal optical measurements

The optical absorbance of $UTa_2O(S_2)_3Cl_6$ from unpolarized light between 3.10 eV (400 nm) and 1.38 eV (900 nm) is displayed in Fig. 3. Absorbance data obtained with polarized light are similar. Two absorbance peaks at 2.04 and 1.76 eV were observed. The presence of these peaks make accurate determination of the optical band gap difficult, but an optical transition at approximately 2.08 eV was determined from a linear regression analysis. This result is consistent with the orange color of $UTa_2O(S_2)_3Cl_6$.

3.5. Theoretical geometric, electronic, and magnetic structure

It did not prove to be possible to obtain enough single crystals of $UTa_2O(S_2)_3Cl_6$ for magnetic measurements. However, an energy

Fig. 3. Single crystal absorbance vs. photon energy (eV) of $UTa_2O(S_2)_3Cl_6$.
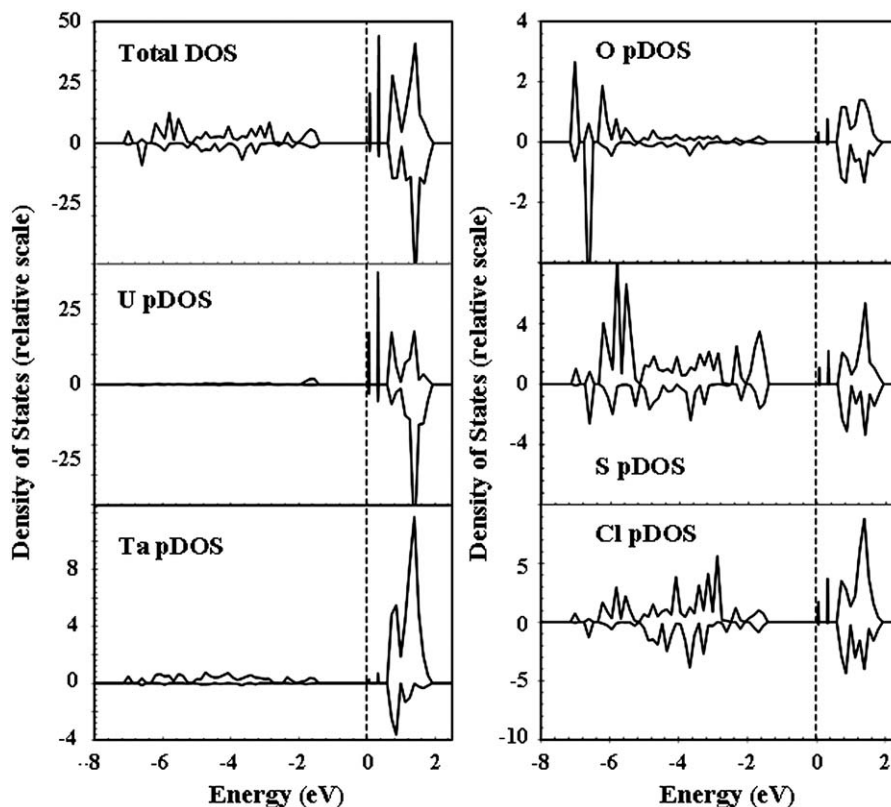
Fig. 4. Total and partial DOS for $UTa_2O(S_2)_3Cl_6$. E_F has been set to 0 eV. Positive DOS represents majority magnetization whereas negative represents minority magnetization.

comparison was made within the LSDA+GGA+SOC method between the two possible magnetic structures. The ferromagnetic alignment of U magnetic moments was found to be 65 meV lower in energy than the antiferromagnetic alignment. For this lowest energy structure, the relaxed positions of the bridging Cl atoms moved the largest amount (0.06 Å) with all other atoms moving less than 0.04 Å. The calculated oxidation state can be written as $U^{4+}/Ta^{5+}/O^{2-}/S^{1.4-}/Cl^{1-}$. The extra $0.4e^-$ on S is likely the result of slight overlap of the R_{WS} sphere with spheres around neighboring U and Ta sites. The total magnetic moment M_J on the U atoms was $1.71\mu_B$ parallel to the axis of magnetization, [001], predominately from the $5f^{2.4}$ with a small $0.03\mu_B$ contribution from the $6d^{0.5}$ electrons. All other atoms had magnetic moments less than $0.02\mu_B$.

The onsite Coulomb correction U_{eff} was varied between -0.5 and 1.8 eV and fit to the experimentally determined optical absorption transitions and band gap. A value of 0.40 eV was found. This value had little effect on the U $5f$ occupancy and only increased the value of M_J on U to $1.74\mu_B$ with a ratio of orbital and spin components, $M_L:M_S = -0.64$. The negative value here is indicative of the antiparallel nature of M_L and M_S. The U magnetization also had small spin and orbital components of magnetization of approximately $0.2\mu_B$ perpendicular to the magnetic field direction. As the onsite Coulomb potential was only applied to the U $5f$-shell the largest effect was the shifting of the $5f$ band energies described below.

3.6. Density of states analysis

The total DOS and partial DOS of each ion calculated with the optimized value of U_{eff} are plotted in Fig. 4. As occurs in many U compounds [53–56], the states surrounding the Fermi energy E_F are dominated by the U $5f$-states with small contributions from the $6d$ states. The determined $5f^{2.4}6d^{0.5}$ electrons on U are located in hybridized $5f$–$6d$ bands at the top of the valence band from approximately -1.5 to -2.0 eV. These states overlap mainly with S $3p$ states but there are also small contributions from all the other states, including those of Ta. In this region the U and Ta states form broad bands that have similar features; this suggests some U/Ta overlap and hence U/Ta interaction in the $UTa_2O(S_2)_3Cl_6$ cluster. The higher energy region between -2.75 and -6.5 eV comprises predominately O, S, and Cl states.

Although many studies have been conducted on the optical transitions of tetravalent U because of its $5f^2$ configuration [57], none has been carried out on such complex a system as the present one. The two peaks in the band gap are identified as majority $5f$ states, but there are small contributions again from U $6d$, S $3p$, and Cl $3p$ states. These f-peaks contain contributions from all M_L component f-orbitals; this suggests considerable exchange, spin–orbit, and crystal-field splitting of the states in this asymmetric heteronuclear coordination environment. It may be too simplistic to describe the observed optical transitions as f–f transitions because there is considerable evidence of $6d$- and $5f$-orbital hybridization and covalent overlap with S and Cl orbitals in both the valence and conduction bands.

4. Supporting material

The crystallographic data for $UTa_2OS_6Cl_6$ have been deposited with FIZ Karlsruhe as CSD number 420806. These data maybe we obtained free of charge by contacting FIZ Karlsruhe at +497247808666 (fax) or crysdata@fiz-karlsruhe.de (e-mail).

Appendix A. Supplementary material

Supplementary data associated with this article can be found in the online version at 10.1016/j.jssc.2009.10.012.

References

[1] A. Müller, R. Jostes, F.A. Cotton, Angew. Chem., Int. Ed. Engl. 19 (1980) 875–882.
[2] U. Müller, V. Krug, Angew. Chem., Int. Ed. Engl. 27 (1988) 293–294.
[3] S.M. Dibrov, J.A. Ibers, C. R. Chimie. 8 (2005) 993–997.
[4] A.F. Cotton, D.O. Marler, W. Schwotzer, Inorg. Chim. Acta 95 (1984) 207–209.
[5] L. Salmon, P. Thuéry, M. Ephritikhine, Polyhedron 25 (2006) 1537–1542.
[6] C.P. Larch, F. Geoffrey, N. Cloke, P.B. Hitchcock, Chem. Commun. (2008) 82–84.
[7] M. Maki, M. Kaiser, A. Zettl, G. Grüner, Solid State Commun. 46 (1983) 497–499.
[8] E.J. Schelter, J.M. Veauthier, J.D. Thompson, B.L. Scott, K.D. John, D.E. Morris, J.L. Kiplinger, J. Am. Chem. Soc. 128 (2006) 2198–2199.
[9] S.A. Kozimor, B.M. Bartlett, J.D. Rinehart, J.R. Long, J. Am. Chem. Soc. 129 (2007) 10672–10674.
[10] P. Jernakoff, C.deM. Bellefon, G.L. Geoffroy, A.L. Rheingold, S.J. Geib, Organometallics 6 (1987) 1362–1364.
[11] S. Blaurock, E. Hey-Hawkins, Eur. J. Inorg. Chem. (2002) 2975–2984.
[12] O. Sigouin, C.N. Garon, G. Delaunais, X. Yin, T.K. Woo, A. Decken, F.-G. Fontaine, Angew. Chem., Int. Ed. Engl. 46 (2007) 4979–4982.
[13] S. Kuwata, S. Kabashima, N. Sugiyama, Y. Ishii, M. Hidai, Inorg. Chem. 40 (2001) 2034–2040.
[14] M.A.F. Hernandez-Gruel, F.J. Lahoz, I.T. Dobrinovich, F.J. Modrego, L.A. Oro, J.J. Pérez-Torrente, Organometallics 26 (2007) 2616–2622.
[15] D.E. Bugaris, J.A. Ibers, J. Solid State Chem. 181 (2008) 3189–3193.
[16] D.L. Gray, L.A. Backus, H.-A. Krug von Nidda, S. Skanthakumar, A. Loidl, L. Soderholm, J.A. Ibers, Inorg. Chem. 46 (2007) 6992–6996.
[17] J.A. Hermann, J.F. Suttle, Uranium(IV) Chloride, in: T. Moeller (Ed.), Inorganic Synthesis, vol. 5, McGraw-Hill Book Company, New York, 1957, pp. 143–145.
[18] Bruker, SMART Version 5.054 Data Collection and SAINT–Plus Version 6.45a Data Processing Software for the SMART System, 2003 (Bruker Analytical X-Ray Instruments, Inc., Madison, WI, USA).
[19] Bruker, APEX2 Version 2009.5-1 and SAINT Version 7.34a Data Collection and Processing Software, 2009 (Bruker Analytical X-Ray Instruments, Inc.: Madison, WI, USA), 2009.
[20] G.M. Sheldrick, Acta Crystallogr. Sect. A: Found. Crystallogr. 64 (2008) 112–122.
[21] L.M. Gelato, E. Parthé, J. Appl. Crystallogr. 20 (1987) 139–143.
[22] K. Mitchell, F.Q. Huang, E.N. Caspi, A.D. McFarland, C.L. Haynes, R.C. Somers, J.D. Jorgensen, R.P. Van Duyne, J.A. Ibers, Inorg. Chem. 43 (2004) 1082–1089.
[23] Materials Data, Inc. JADE8, 2007.
[24] G. Kresse, J. Hafner, Phys. Rev. B 47 (1993) 558–561.
[25] G. Kresse, J. Hafner, Phys. Rev. B 49 (1994) 14251–14271.
[26] G. Kresse, J. Furthmüller, Comput. Mater. Sci. 6 (1996) 15–50.
[27] G. Kresse, J. Furthmüller, Phys. Rev. B 54 (1996) 11169–11186.
[28] G. Kresse, D. Joubert, Phys. Rev. B 59 (1999) 1758–1775.
[29] J. Hubbard, Proc. R. Soc. London, Ser. A 276 (1963) 238–257.
[30] S.L. Dudarev, G.A. Botton, S.Y. Savrasov, C.J. Humphreys, A.P. Sutton, Phys. Rev. B 57 (1998) 1505–1509.
[31] H.J. Monkhorst, J.D. Pack, Phys. Rev. B 13 (1976) 5188–5192.
[32] R.D. Shannon, Acta Crystallogr. Sect. A: Cryst. Phys. Diffr. Theor. Gen. Crystallogr. 32 (1976) 751–767.
[33] G. Henkelman, A. Arnaldsson, H. Jónsson, Comput. Mater. Sci. 36 (2006) 354–360.
[34] J. Yao, D.M. Wells, G.H. Chan, H.-Y. Zeng, D.E. Ellis, R.P. Van Duyne, J.A. Ibers, Inorg. Chem. 47 (2008) 6873–6879.
[35] F. Jellinek, J. Less-Common Met. 4 (1962) 9–15.
[36] V.I. Khitrova, V.V. Klechkovskaya, Z.G. Pinsker, Sov. Phys. Crystallogr. (Engl. Transl.) 17 (1972) 442–447.
[37] V.I. Khitrova, V.V. Klechkovskaya, Sov. Phys. Crystallogr. (Engl. Transl.) 25 (1980) 1169–1175.
[38] G. Hägg, N. Schönberg, Ark. Kemi. 7 (1954) 371–380.
[39] A.C. Gallacher, A.A. Pinkerton, Acta Crystallogr. C 49 (1993) 125–126.

[40] J. Marcoll, A. Rabenau, D. Mootz, H. Wunderlich, Rev. Chim. Miner. 11 (1974) 607–615.
[41] H. Schumann, G. Kociok-Köhn, J. Loebel, Z. Anorg. Allg. Chem. 581 (1990) 69–81.
[42] D. Fenske, A. Grissinger, M. Loos, J. Magull, Z. Anorg. Allg. Chem. 598/599 (1991) 121–128.
[43] H.C. Aspinall, M.R. Tillotson, Inorg. Chem. 35 (1996) 2163–2164.
[44] M. Gasperin, C. R. Hebd. Seances Acad. Sci. 243 (1956) 1534–1536.
[45] M. Gasperin, C. R. Hebd. Seances Acad. Sci. 244 (1957) 1225–1226.
[46] J. Busch, R. Gruehn, Z. Anorg. Allg. Chem. 622 (1996) 640–648.
[47] M. Schleifer, J. Busch, B. Albert, R. Gruehn, Z. Anorg. Chem. 626 (2000) 2299–2306.
[48] H.H. Hill, The early "actinides": the periodic system's f electron transition metal series, in: W.N. Miner (Ed.), Plutonium 1970 and Other Actinides, Vol.vol. 17, The Metallurgical Society of the American Institute of Mining, Metallurgical, and Petroleum Engineers, Inc., New York, 1970, pp. 2–19.
[49] H. Mizoguchi, D. Gray, F.Q. Huang, J.A. Ibers, Inorg. Chem. 45 (2006) 3307–3311.
[50] T. Schleid, G. Meyer, L.R. Morss, J. Less-Common Met. 132 (1987) 69–77.
[51] S. Fiechter, W.F. Kuhs, R. Nitsche, Acta Crystallogr. Sect. B: Struct. Crystallogr. Cryst. Chem. 36 (1980) 2217–2220.
[52] E. Rivard, A.J. Lough, I. Manners, Acta Cryst. Sect. E: Struct. Rep. Online 59 (2003) m239–m240.
[53] V.N. Antonov, B.N. Harmon, A.N. Yaresko, A.Y. Perlov, Phys. Rev. B 59 (1999) 14571–14582.
[54] A.B. Shick, W.E. Pickett, Phys. Rev. Lett. 86 (2001) 300–303.
[55] L.V.S. Pourovskii, M.I. Katsnelson, A.I. Lichtenstein, Phys. Rev. B 72 (2005) 115106/1–115106/8.
[56] P. de la Mora, O. Navarro, J. Phys.: Condens. Matter 20 (2008) 285221/1–285221/6.
[57] G. Liu, J.V. Beitz, Optical spectra and electronic structure, in: L.R. Morss, N.M. Edelstein, J. Fuger (Eds.), The Chemistry of the Actinide and Transactinide Elements, third ed., vol. 3, Springer, Dordrecht, The Netherlands, 2006, pp. 2013–2111.